ChemComm

COMMUNICATION

View Article Online
View Journal

Cite this: DOI: 10.1039/d1cc01438b

Received 17th March 2021,
Accepted 17th June 2021

DOI: 10.1039/d1cc01438b

rsc.li/chemcomm

Effect of silver electrode wetting state on oxygen reduction electrochemistry†

Austin McKee, ‡[a] Avik Samanta, ‡[b] Alan Rassoolkhani,[a] Jonathan Koonce,[a] Wuji Huang,[b] Jacob Fields,[a] Scott K. Shaw, [c] Joseph Gomes, [a] Hongtao Ding *[b] and Syed Mubeen *[a]

Surface wettability plays an important role in heterogeneous electrocatalysis. Here we report a facile laser ablation strategy to directly modify the wettability of the silver catalyst surface and investigate its effect on oxygen reduction reaction (ORR). A broad range tuning of $2e^-/4e^-$ ORR pathways was achieved, with hydrophilic silver surfaces (contact angle (θ_w) 31.1° ± 0.6°) showing high activity and selectivity towards $4e^-$ reduction of oxygen to water.

An abiding goal in electrochemical energy storage and electrosynthetic systems is to design stable electrocatalysts that offer good control over chemical reactivity and product selectivity. Traditionally this has been accomplished by controlling the electronic structure of the electrocatalyst surface by defect engineering, alloying, or doping, to ensure optimal adsorption and desorption of reactant, intermediates, and products.[1–5] Recently, it has been posited that the wettability of the electrocatalyst surfaces can also be used to control the activity and selectivity of chemical transformations involved.[6] The latter has attracted particular attention in three-phase electrochemical systems, wherein a gas-phase reactant, liquid electrolyte, and solid catalyst (electrode) are all in intimate contact.[7–9] The underlying reasons have been mainly attributed to improvements in reactant mass transfer by enriching desired reactants at the electrocatalyst surface7 and inhibiting side reactions to improve product selectivity. In most seminal works, the typical electrode architecture is to have nanostructured catalysts deposited on a hydrophilic or hydrophobic carbon support.[4,5,10] While the above electrode architecture has practical relevance, we envision that the direct tuning of catalyst surface wetting state could decouple other confounding factors such as carbon electrode porosity and mass transport and consequently provide insights on solely how hydrophobicity of the catalyst surface impacts three-phase electrochemical reactions.

Here, through a laser surface nanotexturing process and post-silane treatment, we directly modify the silver electrode surface wettability and investigate its effect on O_2 electroreduction reaction (ORR), a prototypical three-phase reaction of interest for energy conversion and storage applications. Contrary to the other reports, we show that the reaction rates decrease with an increase in catalyst surface hydrophobicity (contact angle (θ_w) 31.1° ± 0.6° to 136.6° ± 1.9°) primarily due to an increase in charge and mass transport resistance at the electrode–electrolyte interface. Notably, the selectivity towards $4e^-$ ORR pathway was high for both hydrophilic (θ_w 31.1° ± 0.6°) and hydrophobic (θ_w 136.6° ± 1.9°) silver electrodes, which we ascribe to different reaction mechanistic pathways at these surfaces. The above findings could shed new insights into the design and fabrication of highly efficient and selective electrocatalysts for various three-phase reactions.

A nanosecond, laser-based, high-throughput, surface nanostructuring (nHSN) process was employed to impart different wettability on the silver electrode surface.[11–13] nHSN is a two-step process (Fig. 1a) where the first step includes surface texturing with infrared Nd:YAG nanosecond pulsed laser (wavelength 1064 nm) under water confinement followed by chemical immersion treatment (CIT) to modify the surface chemistry. Details of the surface processing of the silver samples can be found in the ESI.† To impart hydrophobicity, silver surfaces after laser texturing were immersed in an ethanolic solution of *1H,1H,2H,2H*-perfluorododecyltrichlorosilane [$CF_3(CF_2)_9(CH_2)_2SiCl_3$; 97%], also known as FDDTS. The FDDTS treatment reduces the surface energy of laser-textured silver due to attachment of the low energy functional groups (–CH_2–, –CF_2– and –CF_3) on top of the nanostructures leading to hydrophobicity.[11,14] Silver samples nanostructured with a laser intensity of 8.4 GW cm^{-2} and FDDTS treatment resulted in a contact angle (θ_w) of 136.6° ± 1.9° (Fig. 1b). To achieve hydrophilicity, laser textured silver samples were immersed in an ethanolic solution of 3-cyanopropyltricholosilane [$CN(CH_2)_3SiCl_3$; 97%], also known as CPTS. The CPTS treatment, on the other hand, generates water affinitive polar nitrile (R–C≡N) group on laser-generated Ag nanostructures contributing toward hydrophilicity (Fig. 1b).[15] For example, an 8.4 GW cm^{-2} laser-treated silver sample after CPTS treatment showed a θ_w of

[a] Department of Chemical and Biochemical Engineering, University of Iowa, Iowa City, IA 52242, USA. E-mail: syed-mubeen@uiowa.edu
[b] Department of Mechanical Engineering, University of Iowa, Iowa City, Iowa 52242, USA
[c] Department of Chemistry, University of Iowa, Iowa City, IA 52242, USA

† Electronic supplementary information (ESI) available. See DOI: 10.1039/d1cc01438b

‡ Co-first Author.

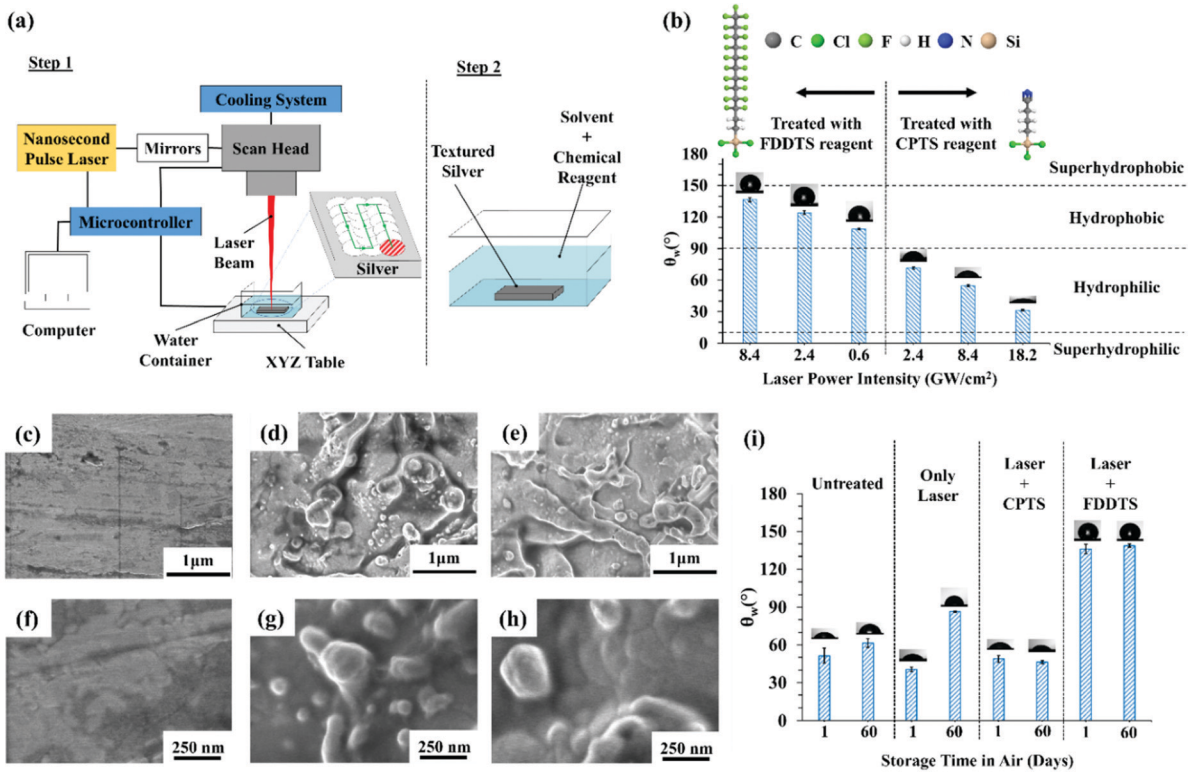

Fig. 1 (a) nHSN process to process silver surface combining nanosecond laser texturing in water confinement (step 1) followed by chemical immersion treatment (step 2); (b) wettability tuning from a hydrophobic range to a hydrophilic range by varying laser power intensity and surface chemistry; low and high-magnification SEM images of hand-polished (c and f), hydrophobic (d and g) and hydrophilic (e and h) silver samples; (i) stability of wettability for nHSN processed silver over a period of 60 days.

54.6° ± 0.9°. Notably, the roughness values measured using a 3D optical white light interferometer were similar for hydrophilic and hydrophobic Ag processed with the same laser power intensity (ESI† Fig. S1). No changes to the intrinsic electronic structures of Ag was also observed after laser and chemical treatment (see ESI† Fig. S2, S4 and S6)

The laser intensity was further prescriptively tuned to vary the wetting state of the electrode surface (Fig. 1b). Both hydrophobicity and hydrophilicity increased with increasing laser intensities. For example, laser-textured FDDTS treated Ag samples showed an increase in θ_w from 108.6° ± 0.9° at 0.6 GW cm^{-2} to 136.6° ± 1.9° at 8.4 GW cm^{-2}, while laser-textured CPTS treated Ag samples showed an increase in hydrophilicity from θ_w = 71.4° ± 1.1° at 2.4 GW cm^{-2} to 31.1° ± 0.6° at 18.2 GW cm^{-2}. This can be ascribed to an increase in nanoscale roughness for samples treated with high laser intensities (ESI† Fig. S3). Scanning electron microscopy images of untreated and 8.4 GW cm^{-2} laser textured hydrophobic and hydrophilic silver electrodes are shown in Fig. 1c–h. The untreated silver electrode (Fig. 1c and f) did not have any surface micro/nanostructures; instead, linear abrasion marks from hand polishing were still observed. On the other hand, both hydrophobic (Fig. 1d and g) and hydrophilic (Fig. 1e and h) showed micro/nanoscale surface features, including various-shaped protrusions and ripples and nanoparticles, generated by the nHSN process. Fig. 1i shows the silver electrodes wetting state stability in the air as a function of time and treatment. Hand-polished silver being an electronegative metal, is intrinsically hydrophilic[16,17] and showed a slight increase in contact angle (from 51.4° ± 6° to 61.3° ± 3.5°) for 60 days storage in ambient conditions. However, the laser-treated electrodes without chemical treatment show a substantial increase in θ_w, almost 2-fold (from 40.5° ± 1.6° to 86.4° ± 0.4°) after 60 days. We attribute this increase in contact angle for laser-textured samples prior to chemical treatment to enhanced adsorption of atmospheric organic constituents and airborne hydrocarbons due to increased surface area from nanoscale features.[18,19] Notably, the laser textured electrodes treated with FDDTS and CPTS showed remarkable stability with less than 4% change in its θ_w when exposed to air over the 60 days observation period. The fluorocarbon and nitrile-terminated surfaces from chemical immersion treatment protected the laser-generated nanostructures from atmospheric organic constituents, thus stabilizing its wetting state.

The silver electrodes with different wetting states were then tested for their electrochemical activity and selectivity for O_2 reduction reaction (ORR). Fig. 2a shows a linear sweep voltammogram (LSV) of silver electrodes with different water contact angles in an O_2 saturated NaOH electrolyte (0.1 M, pH 13). All electrochemical tests were conducted in a three-electrode electrochemical setup with a platinum wire as the counter electrode and Hg|HgO as the reference electrode. Oxygen was purged continuously through the solution at least 30 minutes prior to

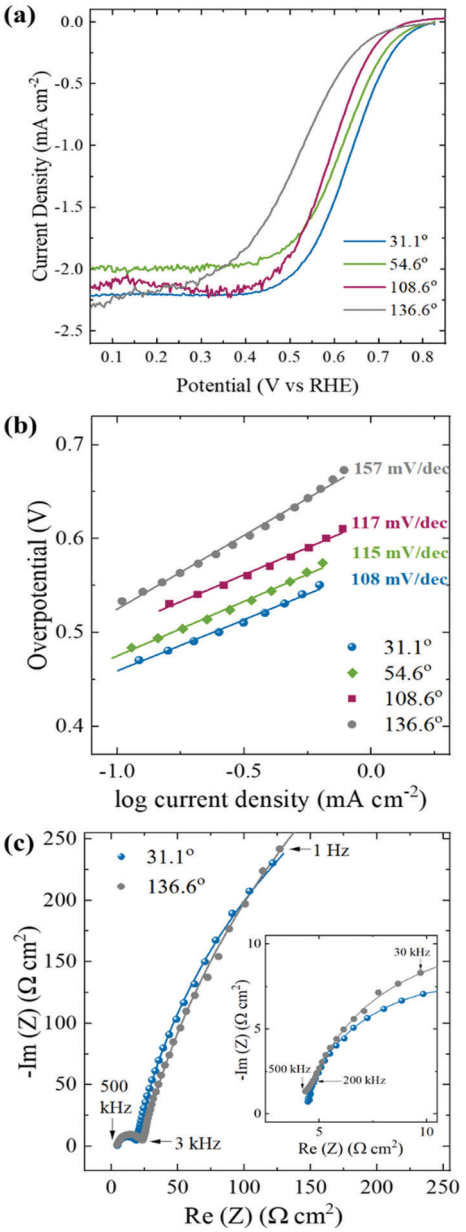

Fig. 2 (a) Linear Sweep Voltammetry at 400 RPM and (b) Tafel Slopes of silver electrodes for four different wetting states. (c) Nyquist plots for hydrophilic (θ_w = 31.1° ± 0.6°) and hydrophobic (θ_w = 136° ± 1.9°) silver electrode at 0.6 V *vs.* RHE. The symbols and the solid lines show the experimental and fitted data, respectively. The inset shows the Nyquist plot at a high-to mid-frequency regime. All measurements were conducted in O_2 saturated 0.1 M NaOH electrolyte.

and throughout the testing process to ensure complete oxygen saturation. The LSV measurements were carried out at a 5 mv s^{-1} scan rate and were repeated until stable voltammograms were obtained. As shown by the LSV, the hydrophilic silver electrodes (θ_w = 31.1° ± 0.6°) exhibited a significant increase in ORR activity compared to hydrophobic electrodes (θ_w = 136.6° ± 1.9°) with more positive onset potential. These are reflected by the half-wave potential ($E_{1/2}$)–the potential at which the current equals one-half of the limiting current – values observed for hydrophilic silver electrodes ($E_{1/2,\ 31.1}^{\circ}$ = 0.64 V *vs.* RHE), which is 120 mV higher than the hydrophobic silver electrodes ($E_{1/2,\ 136.6}^{\circ}$ = 0.52 V *vs.* RHE). This increase in ORR activity of hydrophilic electrodes could be attributed to an increase in kinetic and/or mass transport processes at the electrode–electrolyte interface.

To probe the kinetic effects, Tafel plots were constructed for the kinetically controlled regime (Fig. 2b). The hydrophilic silver electrode showed a lower Tafel slope ($b_{31.1}^{\circ}$ = 108 mV decade^{-1}) and higher exchange current densities ($i_{o,31.1}^{\circ}$ = 1.1 × 10^{-7} A m^{-2}) compared to hydrophobic electrode ($b_{136.6}^{\circ}$ = 157 mV decade^{-1}; $i_{o,136.6}^{\circ}$ = 1.4 × 10^{-8} A m^{-2}), indicating improved intrinsic ORR kinetics with improved electrode wettability. This is contrary to other reports that reported higher activity for hydrophobic electrodes, wherein the typical electrode architecture consisted of nanostructured catalysts loaded on hydrophobic carbon supports.[4,5] We hypothesize that the difference in observation could be due to interference of other effects such as improved mass transport of gaseous reactant in porous carbon electrodes with an increase in hydrophobicity and not solely due to the hydrophobicity of the catalyst alone.

To understand the effect of mass transport processes on ORR activity, potentiostatic electrochemical impedance spectroscopy (PEIS) was carried out at a mixed diffusion-controlled regime (@0.6 V *vs.* RHE) with an initial frequency of 500 kHz to 1 Hz and an amplitude of 20 rms mV as AC excitation signal (Fig. 2c). The Nyquist plot (which represents impedance as a complex number with its real part in the *x*-axis and imaginary part in the *y*-axis) for hydrophilic silver electrodes (θ_w = 31.1° ± 0.6°) showed two semicircles (Fig. 2c, blue trace). The semicircle at the high-mid frequency regime (500 kHz to 3.5 kHz) is indicative of the charge transfer process at the electrode–electrolyte interface, with the diameter of the semicircle representing the charge transfer resistance. The semicircle at the mid-low frequency regime (3.5 kHz to 1 Hz) could be attributed to the O_2 mass transport.[21] Fitting the EIS spectrum for hydrophilic silver (θ_w = 31.1° ± 0.6°) with two RC constants gave us a charge transfer resistance (R_{ct}) value of 14.5 Ω cm^{-2} and an oxygen mass transport resistance (R_{O_2}) of 969 Ω cm^{-2}. Interestingly, the EIS spectrum of the silver electrode with contact angle 136° ± 1.9° showed three distinct regions (Fig. 2c, grey trace). Along with two semicircles that account for charge transport and O_2 mass transport, a 45° straight line at high-frequency region (500 kHz–200 kHz) was observed. The 45° straight line at high frequencies can be attributed to the transport of OH^- ions (R_{OH-})[21] and was only seen for the hydrophobic electrode. Fitting the EIS spectra of the hydrophobic electrode with three RC constants gave us an R_{OH-} of 2.5 Ω cm^{-2}, an R_{ct} of 17.4 Ω cm^{-2} and an R_{O_2} of 1328 Ω cm^{-2} for the hydrophobic electrode. Based on the above observations, we conclude that the significant increase in the ORR activity of the hydrophilic electrode could be attributed to improved Tafel slope and decreased mass transport resistances for O_2 and OH^- ions. To ensure that the wetting state of the silver electrode was maintained, the contact angle measurements were carried out after 2 hours of electrochemical testing (ESI† Fig. S5 and S6). All samples maintained their initial

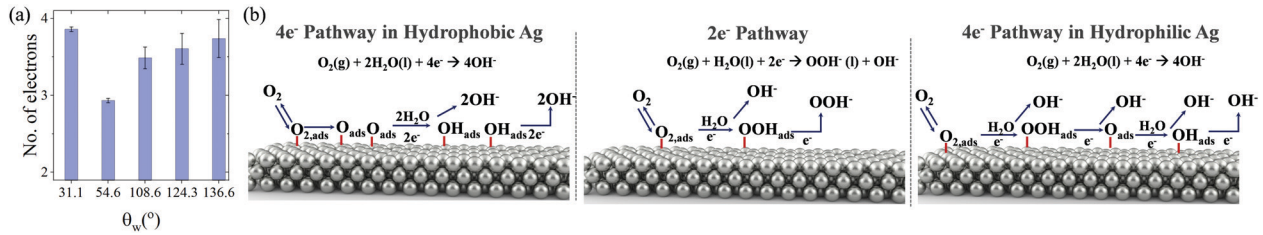

Fig. 3 (a) Average number of electrons per product formed with two electrons forming peroxides and four electrons forming hydroxides and (b) proposed product pathway for hydrophobic (left), hydrophilic (middle), and super hydrophilic (right) samples.

contact angles, indicating that the electrochemistry did not alter the physical and chemical structure of the surface.

To determine the number of electrons utilized for ORR ($4e^-$ for hydroxide formation *versus* $2e^-$ for peroxide formation), Koutecký–Levich (K–L) plots were constructed from LSV's in which the current density and rotational speed are compared at a single potential (ESI† Fig. S7). The silver electrodes were mounted directly on the rotating disk, and LSVs were obtained for five rotational speeds (400, 900, 1600, 2500, and 3600 RPM). The slope of the K–L plot was then used to determine the number of electrons used for the reaction at the tested potential (Fig. 3a). As shown in Fig. 3a, with a decrease in θ_w from 136.6° ± 1.9° to 54.6° ± 0.9°, the electron transfer number decreases from 4 to 3. Remarkably, for the silver electrode with θ_w 31.1° ± 0.6°, the electron number increases back towards 4. Chemical treatment alone did not show any significant changes in ORR activity and product selectivity (ESI† Fig. S8). The mechanistic impact on the electron transfer number as a function of the silver electrode wetting state can be explained by the influence of water on the adsorbed $O_{2,ads}$.[20] The increased selectivity towards $4e^-$ ORR reaction pathway for hydrophobic environment is likely due to the restriction of water access around the active sites that results in the dissociation of adsorbed O_2 to $2O_{ads}$ species which then favors a four electron reduction process as shown in the Fig. 3b left panel. As silver electrode wettability is increased, the adsorbed O_2 undergoes a reduction in the presence of water to form hydroperoxyl species which favors either a two-electron reduction pathway (Fig. 3b middle panel) or a $4e^-$ reduction pathway with increasing water access (Fig. 3b right panel).[4] Density functional theory calculations show that, as the coverage of water around the active site is increased, the dissolution of OOH^- is energetically disfavoured compared to the dissolution of OH^-, increasing selectivity toward the $4e^-$ ORR reaction pathway in the super hydrophilic environment (see ESI† S8). Thus, directly tuning the hydrophobicity/hydrophilicity of the silver electrode could tune the absorbability of the ORR intermediates leading to product tunability (H_2O *vs.* H_2O_2).

In summary, a facile laser nanotexturing process coupled with chemical treatment allowed direct modification of the wetting state of the catalyst surface for investigating the three-phase oxygen reduction reaction. Contrary to other reports, we observed an increase in activity with an increase in catalyst wettability which we ascribe to a decrease in charge transfer and mass-transport resistances at the electrode–electrolyte interface. Both hydrophobic and hydrophilic samples showed high selectivity towards $4e^-$ oxygen reduction pathway, albeit likely due to different mechanistic pathways. The findings indicate that the direct tuning of the catalyst surface wetting state could potentially be used to design high-efficient and selective catalysts for three-phase electrochemical reactions.

The authors gratefully acknowledge the financial support of the National Science Foundation under grant no. CMMI-1762353. A. M also acknowledges the support through HyperSolar Inc., under grant number 18786500 and CRISP funding.

Conflicts of interest

There are no conflicts to declare.

References

1 T. Kumeda, *et al.*, *Nat. Commun.*, 2018, **9**, 4378.
2 Y. Wang, *et al.*, *ACS Appl. Energy Mater.*, 2020, **3**, 9841–9847.
3 M. Tahir, B. Tahir and N. A. S. Amin, *Appl. Catal., B*, 2017, **204**, 548–560.
4 L. Yu, *et al.*, *J. Catal.*, 2011, **282**, 183–190.
5 G. Hao, *et al.*, *Chem. Commun.*, 2015, **51**, 17285.
6 T. Burdyny, *et al.*, *ACS Sustainable Chem. Eng.*, 2017, **5**, 4031–4040.
7 A. Li, *et al.*, *Angew. Chem.*, 2019, **131**, 14691–14697.
8 Z. Xu, *Nano-Micro Lett.*, 2018, **10**, 8.
9 Y. Wang, *et al.*, *Nano Res.*, 2019, **12**(9), 2055–2066.
10 R. Shi, *et al.*, *Nat. Commun.*, 2020, **11**, 3028.
11 Q. Wang, A. Samanta, S. K. Shaw, H. Hu and H. Ding, *Appl. Surf. Sci.*, 2020, **507**, 145136.
12 H. Ding, Q. Wang, A. Samanta and N. Shen, US20190054571A1, 2019.
13 A. Samanta, Q. Wang, S. K. Shaw and H. Ding, *J. Laser Appl.*, 2019, **31**, 022515.
14 A. Samanta, W. Huang, H. Chaudhry, Q. Wang, S. K. Shaw and H. Ding, *ACS Appl. Mater. Interfaces*, 2020, **12**(15), 18032–18045.
15 J. L. Questel, M. Berthelot and C. Laurence, *J. Phys. Org. Chem.*, 2000, **13**, 347–358.
16 M. A. Osman and B. A. Keller, *Appl. Surf. Sci.*, 1996, **99**, 261–263.
17 G. Valette, *J. Electroanal. Chem. Interfacial Electrochem.*, 1982, **139**, 285–301.
18 A. Samanta, Q. Wang, S. K. Shaw and H. Ding, *Mater. Des.*, 2020, **192**, 108744.
19 J. Long, P. Fan, M. Zhong, H. Zhang, Y. Xie and C. Lin, *Appl. Surf. Sci.*, 2014, **311**, 461–467.
20 S. Bhatia, *Introduction to Pharmaceutical Biotechnology*, 2018, vol. 2, pp. 1–29.
21 T. E. Springer, T. A. Zawodzinski, M. S. Wilson and S. Gottesfeld, *J. Electrochem. Soc.*, 1996, **143**, 587.

